Journal of Materials Chemistry A

Accepted Manuscript

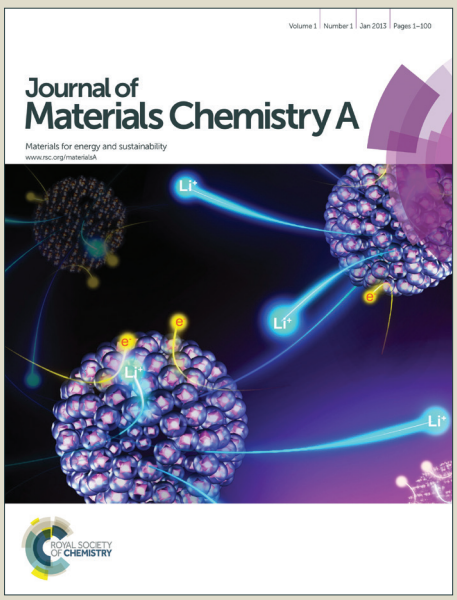

ROYAL SOCIETY OF CHEMISTRY

www.rsc.org/materialsA

Cite this: DOI: 10.1039/c0xx00000x

www.rsc.org/xxxxxx

ARTICLE TYPE

Porous Perovskite Calcium-Manganese Oxide Microspheres as Efficient Catalyst for Rechargeable Sodium-Oxygen Batteries

Yuxiang Hu, Xiaopeng Han, Qing Zhao, Jin Du, Fangyi Cheng and Jun Chen*

Received (in XXX, XXX) Xth XXXXXXXXX 20XX, Accepted Xth XXXXXXXXX 20XX

DOI: 10.1039/b000000x

We report herein the preparation of porous $CaMnO_3$ microspheres and their electrochemical catalytic performance as cathode for rechargeable sodium–oxygen ($Na-O_2$) batteries. In ether-based electrolyte, $CaMnO_3$/C cathode exhibits a high discharge capacity of 9560 mAh g^{-1} at a current density of 100 mA g^{-1}, high rate capability (capacity of 1940 mAh g^{-1} at 1000 mA g^{-1}), and considerable cyclability up to 80 cycles. Two discharged species of NaO_2 and Na_2O_2 are detected at the discharged state. The remarkable electrocatalytic activity of $CaMnO_3$ both for oxygen reduction reaction (ORR) and for oxygen evolution reaction (OER) is attributed to the porous micro-nanostructures in stable ether-based electrolyte.

Over the last decade, rechargeable metal–air batteries have received growing interest because of their significantly higher theoretical energy density than traditional rechargeable metal-ion batteries.[1-6] Particularly, rechargeable sodium–oxygen batteries (with theoretical energy density of about 1600 Wh kg^{-1}) are attractive as sodium shows analogous physicochemical properties to the prevailing lithium. Meanwhile, rechargeable sodium–oxygen batteries show prominent advantages of inexhaustible and ubiquitous resource.[7-9] Similar to the case of rechargeable Li–O_2 system, the discharge product in rechargeable Na–O_2 cell deposits on the electrode surface. Therefore, the cell performance depends critically on the properties of cathode material such as activity, morphology, porosity, conductivity, and specific surface area.[10-15] Recently, various catalysts have been developed to accelerate the sluggish oxygen reduction reaction (ORR) and oxygen evolution reaction (OER) kinetics in rechargeable Na–O_2 batteries.[16-19] These catalysts are mainly based on carbonaceous materials such as carbon fiber,[5] graphene nanosheets,[17] and nitrogen-doped graphene.[19] Transition metal oxides (such as manganese oxides) represent another class of oxygen electrocatalysts for their advantages of low cost, high abundance, environmentally benign and considerable catalytic activity in both aqueous and aprotic electrolytes.[20-35] Recently, we have revealed that composite manganese oxides (i.e., $CaMnO_3$) exhibit enhanced ORR/OER activity in comparison with binary manganese oxides.[36-39] Aiming at exploring efficient cathode catalysts composed of earth-abundant and inexpensive elements for rechargeable Na–O_2 technologies, it deserves special attention to make use of metal oxides in this emerging battery chemistry. However, to the best of our knowledge, there is rarely attempt to employ transition metal oxide catalytic materials in rechargeable Na–O_2 batteries. Herein, we report the preparation of perovskite $CaMnO_3$ oxide with micro-nano structure and its application as an efficient electrocatalyst for rechargeable Na–O_2 batteries. Porous $CaMnO_3$ microspheres were synthesized by simple thermal decomposition of carbonate precursors. When applied as cathode catalyst, $CaMnO_3$–based electrode exhibits a high discharge capacity of 9560 mAh g^{-1} and a respectable cyclability (up to 80 cycles).

Porous $CaMnO_3$ microspheres were synthesized by simply firing the solid-solution precursor of $CaMn(CO_3)_2$ in air (Details described in Electronic Supplementary Information, ESI).[40] Figure 1a shows the powder X-ray diffraction (XRD) pattern and the corresponding Rietveld refinement of the as-prepared $CaMnO_3$. The diffraction peaks could be readily indexed to the orthorhombic $CaMnO_3$ (Joint Committee on Powder Diffraction Standards, JCPDS card no. 76-1132). The Rietveld refinement gives the calculated cell parameters of a = 5.279 Å, b = 7.452 Å, and c = 5.287 Å, in good agreement with the standard values. As shown in the inset of Figure 1a, $CaMnO_3$ adopts the typical perovskite structure (space group: *Pnma*), which is composed of the framework of corner-sharing MnO_6 octahedra with Mn atoms locating at the center and Ca atoms occupying the inter-octahedral sites.

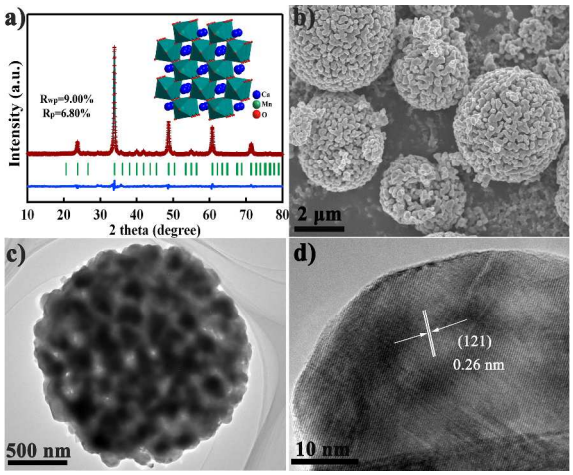

Fig. 1 (a) Rietveld refined XRD pattern of porous $CaMnO_3$ with experimental data (red dots), calculated profile (cyan line), allowed Bragg reflections (green vertical line) and the difference curve (blue line). Inset shows the crystal structure of $CaMnO_3$. (b) SEM image, (c) TEM and (d) HRTEM images of synthesized $CaMnO_3$.

Typical scanning electron microscopy (SEM) image (Figure 1b) presents the hierarchical microspheres of the as-synthesized oxide sample with diameter of 2.0–4.0 μm. The microspheres are composed of aggregated nanoparticles, and the morphology maintains similar spherical shape of the carbonate precursor (Figure S1, ESI). The size of the microspheres could be adjusted by varying experimental conditions such as reaction temperature and carbonate precipitant amount. Higher temperature and more CO_3^{2-} lead to $CaMnO_3$ microspheres with smaller size (Figure S2, ESI). Transmission electron microscopy (TEM) image (Figure 1c) further reveals the presence of pores surrounded by the interconnected nanoparticles. From the high-resolution TEM image (Figure 1d), the neighboring interlayer distance is measured to be 0.26 nm, which is consistent with the (121) plane of $CaMnO_3$ and further evidences the perovskite phase. The Brunauer-Emmett-Teller (BET) specific surface area is determined to be 11.8 m^2 g^{-1} by N_2 adsorption-desorption isotherms (Figure S3, ESI).

Figure 2 displays the electrocatalytic performance of the $CaMnO_3$–based and Super P-based electrodes in rechargeable Na–O_2 cells with the electrolyte of tetraethylene glycol dimethyl ether (TEGDME). At a fixed current density of 100 mA g^{-1}, $CaMnO_3$/C cathode exhibits an extremely high capacity of 9560 mAh g^{-1}, which is much larger than the value of pure Super P cathode (3870 mAh g^{-1}) (Figure 2a). The charging off-voltages were all set at a relatively high value of 4.0 V to completely decompose the discharge products on the cathodes. The $CaMnO_3$/C electrode efficiently enhances the coulombic efficiency (95% for $CaMnO_3$/C cathode and 91% for Super P electrode) and reduces the overpotential of rechargeable Na–O_2 cells. The discharge plateau of the cell with $CaMnO_3$ cathode is 2.2 V, about 0.2 V higher than that of Super P-based electrode. Two charging platforms are observed at 2.8 V and 3.5 V, respectively, which are also lower than that for Super P. These discharge-charge curves are different from those of rechargeable Na–O_2 batteries previously reported using carbonate-based electrolyte (Figure S4, ESI). The plateaus of the charge-discharge curves are also confirmed by cycled voltammograms (CV) profiles (Figure 2b, and Figure S5 in ESI). Compared with carbon-only electrode, $CaMnO_3$/C electrode shows a higher cathodic peak position, a lower anodic onset potential and much larger cathodic and anodic currents. These results clearly demonstrate superior catalytic performance of $CaMnO_3$ towards dual ORR/OER in rechargeable Na–O_2 batteries based on ether electrolyte.

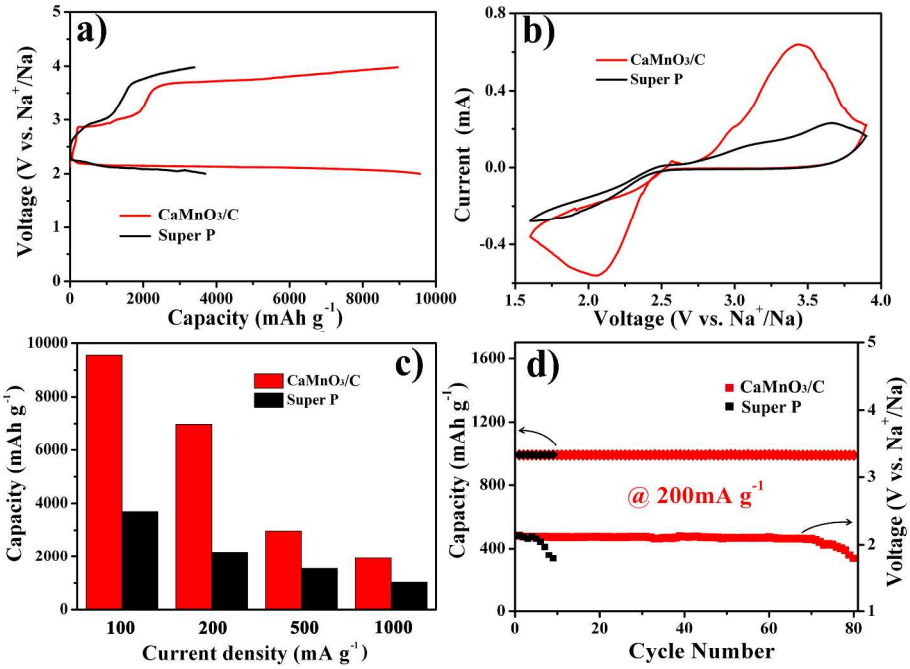

Fig. 2 (a) Discharge–charge curves of $CaMnO_3$/C and Super P electrodes in rechargeable Na–O_2 batteries at a current density of 100 mA g^{-1}, (b) CV curves in $NaSO_3CF_3$/TEGDME electrolyte at a scan rate of 0.1 mV s^{-1}, (c) discharge capacities at different current densities, and (d) cycling performance with a restriction capacity of 1000 mAh g^{-1} and the resulting cut-off discharging voltage. All the capacities and current densities are based on the weight of carbon involved in the electrodes.

The rate capability of the as-prepared catalysts was investigated at different current densities (Figure 2c and Figure S6). The rechargeable Na–O_2 cell with $CaMnO_3$/C delivers much higher capacity and more positive discharge plateau than the counterpart Super P at all current densities. Specifically, even under a high current density of 1000 mA g^{-1}, the $CaMnO_3$/C-based battery exhibits a discharge capacity of 1940 mAh g^{-1}, which is approximately two times higher than that for Super P electrode (1027 mAh g^{-1}). The cycling performance of the assembled batteries were investigated with the discharge capacity restriction of 1000 mAh g^{-1} at a current density of 200 mA g^{-1} (Figure 2d, and Figure S7 in ESI). Controlling the depth of discharge is favorable to suppress the aggregation of insulating discharge product and thus benefits the cell reversibility. The $CaMnO_3$/C cathode accomplishes 80 cycles circulation with stable discharging terrace (>1.85 V), while the pure carbon

cathode can merely sustain less than 10 cycles (Figure 2d), indicating considerable reversible reaction during the discharge-charge process over the $CaMnO_3$/C electrocatalyst. The electrochemical performance of $CaMnO_3$ presented in this study is among the best results reported for rechargeable Na–O_2 batteries based on other cathode catalysts.[16, 17, 19] The insufficient decomposition of the discharge productions along with the increased battery resistance (Figure S8 and Figure S9, ESI) leads to the decay of $CaMnO_3$/C batteries after 80th cycle.

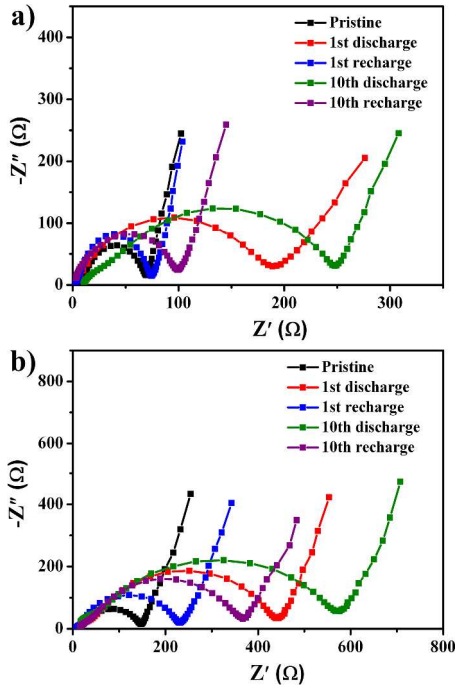

Fig. 3 Electrochemical impedance spectra (EIS) of (a) $CaMnO_3$/C and (b) Super P of discharged/recharged cathodes of the pristine state, and after the 1st and 10th cycles.

The relative reversibility of $CaMnO_3$/C cathode is further verified by the measurements of electrochemical impedance spectroscopy (EIS) (Figure 3). After the 1st discharging, the charge transfer resistance (R_{ct}) of both $CaMnO_3$/C-based and carbon-based batteries increases (from 70 Ω at pristine to 189 Ω after discharged for $CaMnO_3$/C and from 150 Ω at pristine to 443 Ω after discharged for Super P, respectively), which is caused by the formation of nonconductive discharge products on the electrode surface. After the 1st recharging, the R_{ct} of the $CaMnO_3$/C-based battery reveals good recovery (76 Ω vs. 70 Ω) (Figure 3a), whereas that of carbon-only electrode is hard to be recovered (233 Ω vs. 150 Ω) (Figure 3b). This phenomenon becomes much more apparent after the 10th cycle. Compared with Super P electrode, the increase of charge transfer resistance is much slower in $CaMnO_3$/C electrode. Therefore, the $CaMnO_3$/C cathode is again proved to be an effective catalyst for the reversibility electrochemical processes.

To investigate the discharge-charge mechanism of the operated rechargeable Na–O_2 cells, Raman and XRD measurements were performed at four different stages of the first cycle at a current density of 100 mA g^{-1} (Figure 4). Four points, namely the pristine, fully discharged to 2.0 V, charged to 3.0 V, and charged to 3.9 V, are selected as the feature states. Both Raman spectra (Figure 4a) and XRD patterns (Figure 4b) reveal the fully discharged products of sodium superoxide (NaO_2) and sodium peroxide (Na_2O_2) in the TEGMDE-based electrolyte. In contract, in the carbonate-based electrolyte, Na_2O_2 is detected (Figure S10, ESI) as the only discharge product, which has also been proved in previous articles.[17, 19] After charging to 3.0 V, the sodium superoxide vanishes while the sodium peroxide remains. This indicates that the decomposition potential of NaO_2 is below 3.0 V, which is in consistent with previous results.[13, 15] Furthermore, the sodium peroxide disappears after charging to 3.9 V. Therefore, both NaO_2 and Na_2O_2 are observed in the discharged products after discharging to 2.0 V and they are gradually oxidized at two different potentials (about 2.8 V for NaO_2 and 3.5 V for Na_2O_2 from the charging curves) during the following charge process.

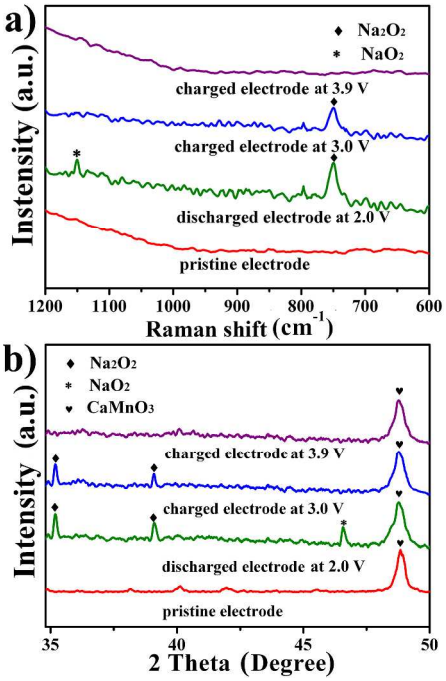

Fig. 4 (a) Raman spectra and (b) XRD patterns of the electrodes at four selected stages: the pristine state, discharging to 2.0 V, charging to 3.0 V and charging to 3.9 V after 1st cycle.

From the similar standard potentials and thermodynamic data of the two reactions, $Na + O_2 = NaO_2$ (E^o = 2.26 V, $\Delta G°$ = –437.5 kJ mol^{-1}) and $2Na + O_2 = Na_2O_2$ (E^o = 2.33 V, $\Delta G°$ = –449.7 kJ mol^{-1}),[5, 41] it can be deduced that the discharged products feasibly contain a mixture of NaO_2 and Na_2O_2 after discharging to 2.0 V vs. Na^+/Na. The electrodes at four discharge/charge states were also analyzed using SEM (Figure 5). Compared with the initial loose and porous morphology (Figure 5a), the insoluble discharge species with cubic-like morphology precipitate on the surface of the cathode after discharging (Figure 5b). Notablely, the cubic-like morphology disappears after recharging to 3.0 V (Figure 5c). Furthermore, energy-dispersive spectroscopy (EDS) of single cubic-like particle displays that the elements ratio of O to Na is around 2:1 (Figure S11a, ESI), which is consistent with previous characterizations about generation of cubic shape NaO_2 in rechargeable Na–O_2 system.[5, 15, 42] The mole ratio of the oxygen

to sodium in other position over the electrode (Figure S11b, ESI) is about 1:1. This confirms the above discharge products of the mixtured sodium oxides (Na_2O_2 and NaO_2) as detected in Raman and XRD characterizations. After fully recharging to 3.9 V, the electrode essentially recovers to the pristine state (Figure 5d), further confirming reversible reaction over the $CaMnO_3$/C cathode catalyst.

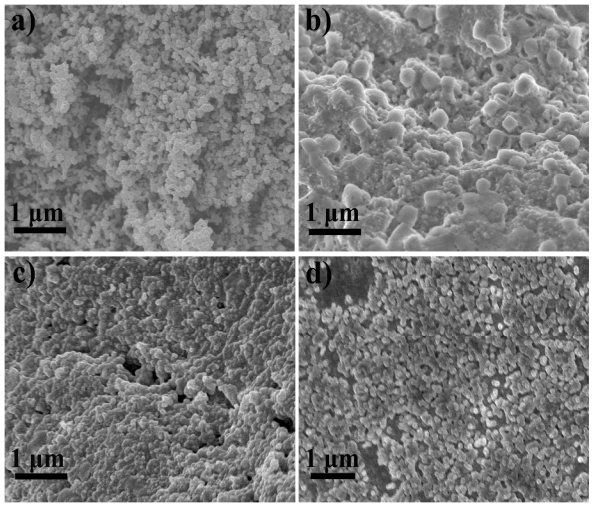

Fig. 5 SEM images of the $CaMnO_3$/C electrode at different stages in the first cycle: (a) pristine, (b) after discharging to 2.0 V, (c) after charging to 3.0 V, and (d) after charging to 3.9 V.

In summary, we report the synthesis of porous $CaMnO_3$ microspheres and the application as a new cathode electrocatalyst in rechargeable sodium–oxygen batteries. Porous micro-nanostructured $CaMnO_3$ electrode delivered a high specific capacity of 9560 mAh g^{-1}, a high rate capacity (1940 mAh g^{-1} at current density of 1000 mA g^{-1}) and enhanced cyclability (up to 80 cycles). The micro-nano structure of porous $CaMnO_3$ microspheres provides abundant active sites for bifunctional ORR/OER and effective space for the accommodation of NaO_2 or Na_2O_2. This work indicates the promising applicability of $CaMnO_3$ as abundant, low-cost, and efficient catalytsts for rechargeable sodium–oxygen batteries.

Acknowledgements

This work was supported by the National 973 (Grant No. 2011CB935900), NSFC (Grant No. 21231005 and 21232101), and MOE (Grant No. B12015 and ACET-13-0296).

Notes and references

Key Laboratory of Advanced Energy Materials Chemistry (Ministry of Education), Collaborative Innovation Center of Chemical Science and Engineering, Nankai University, Tianjin 300071, China. Fax: 86-22-23504486; Tel: 86-22-23506808.
E-mail: chenabc@nankai.edu.cn
Y. H. and X. H. contribute equally to this work.

‡Electronic supplementary information (ESI) available: Detailed synthesis method, material characterization, cell assembly procedures, electrochemical tests, XRD, BET, SEM, Raman, and EDS images, N_2 adsorption-desorption curve, and additional electrochemical results. See DOI:

1 Z. Q. Peng, S. A. Freunberger, Y. Chen, P. G. Bruce, *Science* 2012, **337**, 563-566.
2 F. Y. Cheng and J. Chen, *Chem. Soc. Rev.*, 2012, **41**, 2172-2192.
3 Z. L. Wang, D. Xu, J. J. Xu and X. B. Zhang, *Chem. Soc. Rev.*, 2014, **43**, 7746-7786.
4 T. R. Zhang, Z. L. Tao and J. Chen, *Mater. Horiz.*, 2014, **1**, 196-206.
5 P. Hartmann, C. L. Bender, M. Vračar, A. K. Dürr, A. Garsuch, J. Janek, P. Adelhelm, *Nat. Mater.*, 2012, **12**, 228-232.
6 F. Y. Cheng and J. Chen, *Nat. Chem.*, 2012, **4**, 962-963.
7 B. L. Ellis and L. F. Nazar, *Curr. Opin. Solid State Mater. Sci.*, 2012, **16**, 168-177.
8 S. Kang, Y. Mo, S. P. Ong and G. Ceder, *Nano. Lett.*, 2014, **14**, 1016-1020.
9 P. Hartmann, D. Grübl, H. Sommer, J. Janek, W. G. Bessler and P. Adelhelm, *J. Phys. Chem. C*, 2014, **118**, 1461-1471.
10 F. Y. Cheng and J. Chen, *Acta Chim. Sinica*, 2013, **71**, 473-477.
11 B. D. Bhatt, H. Geaney, M. Nolan and C. O'Dwyer, *Phys. Chem. Chem. Phys.*, 2014, **16**, 12093-12130.
12 Y. Cao, M. S. Zheng, S. R. Cai, X. D. Lin, C. Yang, W. Q. Hu and Q. F. Dong, *J. Mater. Chem. A*, 2014, DOI: 10.1039/c4ta04488f.
13 S. K. Das, S. Lau and L. Archer, *J. Mater. Chem. A*, 2014. DOI : 10.1039/c4ta02176b.
14 E. Peled, D. Golodnitsky, H. Mazor, M. Goor and S. Avshalomov, *J. Power Sources*, 2011, **196**, 6835-6840.
15 P. Hartmann, C. L. Bender, J. Sann, A. K. Dürr, M. Jansen, J. Janek and P. Adelhelm, *Phys. Chem. Chem. Phys.*, 2013, **15**, 11661-11672.
16 Q. Sun, Y. Yang and Z. W. Fu, *Electrochem. Commun.*, 2012, **16**, 22-25.
17 W. Liu, Q. Sun, Y. Yang, J. Y. Xie and Z. W. Fu, *Chem. Commun.*, 2013, **49**, 1951-1953.
18 J. Kim, H. D. Lim, H. Gwon and K. Kang, *Phys. Chem. Chem. Phys.*, 2013, **15**, 3623-3629.
19 Y. L. Li, H. Yadegari, X. F. Li, M. N. Banis, R. Y. Li and X. L. Sun, *Chem. Commun.*, 2013, **49**, 11731-11733.
20 L. Zhang, S. L. Zhang, K. J. Zhang, G. J. Xu, X. He, S. M. Dong, Z. H. Liu, C. S. Huang, L. Gu and G. L. Cui, *Chem. Commun.*, 2013, **49**, 3540-3542.
21 F. Y. Cheng, J. Shen, B. Peng, Y. D. Pan, Z. L. Tao and J. Chen, *Nat. Chem.*, 2010, **3**, 79-84.
22 K. J. Zhang, L. X. Zhang, X. Chen, X. He, X. G. Wang, S. M. Dong, P. X. Han, C. J. Zhang, S. Wang, L. Gu and G. L. Cui, *J. Phys. Chem. C*, 2013, **117**, 858-865.
23 X. P. Han, T. R. Zhang, J. Du, F. Y. Cheng and J. Chen, *Chem. Sci.*, 2013, **4**, 368-376.
24 K. Zhang, X. P. Han, Z. Hu, X. L. Zhang, Z. L. Tao and J. Chen, *Chem. Soc. Rev.*, 2014. DOI: 10.1039/c4cs00218k.
25 X. P. Han, F. Y. Cheng, T. R. Zhang, J. G. Yang, Y. X. Hu and J. Chen, *Adv. Mater.*, 2014, **26**, 2047-2051.
26 C. Z. Yuan, H. B. Wu, Y. Xie and X. W. Lou, *Angew. Chem. Int. Ed.*, 2014, **53**, 1488-1504.
27 F. Y. Cheng, T. R. Zhang, Y. Zhang, J. Du, X. P. Han and J. Chen, *Angew. Chem. Int. Ed.*, 2013, **52**, 2474-2477.
28 Q. Jin, L. K. Pei, Y. X. Hu, J. Du, X. P. Han, F. Y. Cheng, J. Chen, *Acta Chim. Sinica*, 2014, **72**, 920-926.
29 J. Du, F. Y. Cheng, S. W. Wang, T. R. Zhang and J. Chen, *Sci. Rep.*, 2014, **4**, 4386.
30 Y. Cao, X. G. Lin, C. L. Zhang, C. Yang, Q. Zhang, W. Q. Hu, M. S. Zheng and Q. F. Dong, *RSC Adv.*, 2014, **4**, 30150-30155.
31 F. Y. Cheng, Y. Su, J. Liang, Z. L. Tao and J. Chen, *Chem. Mater.*, 2010, **22**, 898-905.
32 X. D. Huang, B. Sun, D. W. Su, D. Y. Zhao and G. X. Wang, *J. Mater. Chem. A*, 2014, **2**, 7973-7979.
33 T. R. Zhang, F. Y. Cheng, J. Du, Y. X. Hu and J. Chen, *Adv. Energy Mater.*, 2014, DOI: 10.1002/aenm.201400654.
34 B. Peng and J. Chen, *Coord. Chem. Rev.*, 2009, **253**, 2805-2813.
35 J. Liang, R. F. Zhou, X. M. Chen, Y. H. Tang and S. Z. Qiao, *Adv. Mater.*, 2014, **26**, 6074-6079.
36 J. Du, Y. D. Pan, T. R. Zhang, X. P. Han, F. Y. Cheng and J. Chen, *J. Mater. Chem.*, 2012, **22**, 15812-15818.
37 X. P. Han, Y. X. Hu, J. G. Yang, F. Y. Cheng and J. Chen, *Chem. Commun.*, 2014, **50**, 1497-1499.

38 M. M. Najafpour, T. Ehrenberg, M. Wiechen and P. Kurz, *Angew. Chem. Int. Ed.*, 2010, **49**, 2233-2237.
39 J. Du, T. R. Zhang, F. Y. Cheng, W. S. Chu, Z. Y. Wu and J. Chen, *Inorg. Chem.*, 2014, **53**, 9106-9114.
40 H. S. Horowitz, and J. M. Longo, *Inorg. Synth.* **1983**, *22*, 68-72.
41 C. L. Bender, P. Hartmann, M. Vračar, P. Adelhelm and J. Janek, *Adv. Energy Mater.*, 2014, DOI: 10.1002/aenm.201301863.
42 B. Lee, D. H. Seo, H. D. Lim, I. Park, K. Y. Park, J. Kim and K. Kang, *Chem. Mater.*, 2014, **26**, 1048-1055.

TOC

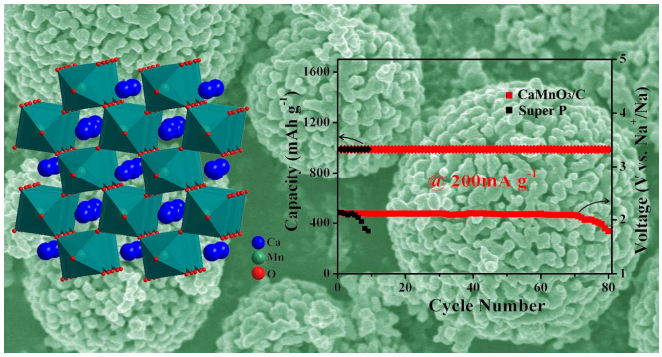

Porous micro-nanostructured $CaMnO_3$ electrode delivered a high specific capacity, high rate capacity and enhanced cyclability in rechargeable sodium–oxygen batteries.